



## Modelling the sensing radius of a coaxial probe for dielectric characterisation of biological tissues

Title	Modelling the sensing radius of a coaxial probe for dielectric characterisation of biological tissues
Author(s)	La Gioia, Alessandra;O'Halloran, Martin;Porter, Emily
Publication Date	2018-08-22
Publisher	Institute of Electrical and Electronics Engineers
Repository DOI	<a href="https://doi.org/10.1109/ACCESS.2018.2866703">10.1109/ACCESS.2018.2866703</a>

# Modelling the sensing radius of a coaxial probe for dielectric characterisation of biological tissues

Alessandra La Gioia<sup>1</sup>, Member, IEEE, Martin O'Halloran<sup>1</sup>, Member, IEEE, and Emily Porter<sup>1</sup>, Member, IEEE

<sup>1</sup>Translational Medical Device Laboratory, National University of Ireland Galway, Galway, Ireland

Corresponding author: Alessandra La Gioia (e-mail: a.lagioia@nuigalway.ie).

The research leading to these results has received funding from the European Research Council under the European Union's Horizon 2020 Programme/ ERC Grant Agreement BioElecPro n. 637780. This work was also supported by Science Foundation Ireland (SFI) (grant number 15/ERCS/3276), and the Hardiman Research Scholarship from the National University of Ireland Galway.

**ABSTRACT** The open-ended coaxial probe is the most common measurement tool used to dielectrically characterise biological tissues. Most healthy and malignant biological tissues are macroscopically heterogeneous, with the exception of a few tissues, such as liver. Heterogeneous biological samples are dielectrically characterised by defining the dielectric properties of each tissue type constituting the sample. In order to accurately characterise a specific tissue type with a coaxial probe, it is fundamental that only the tissue of interest is contained within the probe sensing volume, which is defined by the sensing radius and sensing depth. In the literature, several studies have investigated the sensing depth with bilayer or multilayer heterogeneous tissues. However, in this work, we examine the sensing radius through concentrically heterogeneous tissues. In particular, samples composed of two different concentric tissues were modelled to estimate the minimum width of the homogenous tissue region required to accurately acquire the corresponding dielectric properties. As recent studies have indicated that the sensing radius depends on the dielectric properties of the interrogated tissue, in this study, the sensing radius of a coaxial probe has been numerically quantified across a wide range of scenarios, involving different tissues with varying dielectric contrasts. The numerical results indicate that: i) the sensing radius increases with the contrast in permittivity between the constituent tissues; and ii) the sensing radius is highly dependent on the permittivity of the tissue closest to the inner conductor of the probe. Lastly, the numerical outcome has been confirmed with dielectric measurements performed on animal tissues.

**INDEX TERMS** Biological tissues, coaxial probe, dielectric measurement, electromagnetic simulations, sensing radius.

## I. INTRODUCTION

Knowledge of the dielectric properties of biological tissues is fundamental for the design of promising diagnostic and therapeutic electromagnetic (EM) techniques, such as microwave (MW) imaging and ablation. These technologies are often based on the assumption that there is a contrast in the dielectric properties of different tissue types. For instance, the dielectric properties of each tissue and the magnitude of the contrast between them quantify the minimum operating requirements of MW imaging systems [1], [2]. In addition, the contrast of dielectric properties in healthy and tumour tissues permits targeting malignant tissues while preserving surrounding healthy tissues in MW ablation treatment [3], [4]. For this reason, it is important to accurately determine the dielectric properties of biological tissues [5].

The dielectric properties of tissues, defined by the relative permittivity,  $\epsilon_r$ , and conductivity,  $\sigma$ , are commonly measured using an open-ended coaxial probe [6]–[9]. Dielectric measurement with the coaxial probe is based on the assumption that the measured sample is homogeneous and has infinite size in the transverse and longitudinal directions [10]. In practice, all samples have limited size. In addition, biological tissues generally show heterogeneous structures, which further complicate dielectric measurements with a coaxial probe.

Generally, heterogeneous biological tissue samples are dielectrically characterised by determining the dielectric properties of each tissue type constituting the sample [11], [12]. To accurately measure the dielectric properties of each tissue type, it is fundamental that the tissue of interest is the

only tissue type interrogated by the probe, i.e., the only tissue type present within the sensing volume of the probe.

The sensing volume of the probe consists of the sensing radius, along the transverse direction, and the sensing depth, along the longitudinal direction. Knowledge of the sensing radius and depth allows definition of the minimum width and thickness, respectively, of the homogeneous tissue that can be accurately dielectrically characterised [10]. In fact, if the width (or thickness) of the homogeneous tissue is smaller than the probe sensing radius (or depth), the dielectric properties of the tissue of interest are not accurate, since the properties are affected by other tissues or materials surrounding the tissue of interest. On the other hand, if only the homogeneous tissue region is contained within the probe sensing volume, the dielectric properties of the homogeneous tissue are accurately measured. Therefore, knowledge of sensing radius and depth is fundamental in order to characterise homogeneous tissue types within heterogeneous tissue samples.

To date, many studies have investigated the sensing depth with bilayer or multilayer tissues [13]–[17]. Therefore, in this work, the sensing radius is investigated with concentric samples composed of two different tissues. Recently, initial studies have investigated the sensing radius [18], [19]. Specifically, in [18], the maximum sensing radius of the Keysight slim form probe [20], the most commonly used probe for both *in vivo* and *ex vivo* measurements [12], [21], [22], was quantified through custom dielectric experiments and numerical simulations involving (non-biological) concentric samples consisting of saline solution and Teflon. Furthermore, in [19], the sensing radius of the same slim form probe was quantified with measurements on porcine tissue, and the outcome suggested that the sensing radius depends not only on the probe geometry and materials but also on the dielectric properties of the tissues constituting the interrogated sample.

Thus, in order to complete the characterisation of the sensing radius of the Keysight slim form probe, in this study, the interaction between this probe and concentric biological tissues, with different dielectric properties and contrasts, is investigated to analyse how the sensing radius depends on the dielectric properties of the interrogated biological tissues. In this way, the minimum width of homogeneous tissue region is quantified for a wide range of different tissue types.

In this study, numerical simulations were executed across the range of 2 to 6 GHz, which is the operating frequency of many MW imaging systems and MW ablation applicators [1], [2], [23], [24]. This study focuses on simulation data in order to have a controlled range in the concentric tissue structure and dielectric properties of the tissues investigated, to enable thorough estimation of the sensing radius in different circumstances. However, the numerical outcome has been confirmed by dielectric measurements performed on animal tissues.

This paper is organised as follows. In Section II, the design of the study is detailed and motivated; and in

Section III, the numerical results are reported and then confirmed by experiments on animal tissues. Finally, in Section IV, the experimental outcomes are summarised.

## II. METHODOLOGY

### A. SIMULATION MODEL AND TISSUE PROPERTIES

Measurements with the Keysight slim form probe were simulated numerically on biological tissues with a heterogeneous structure that enables estimation of the sensing radius. The slim form probe was modelled numerically in our previous studies [18], [19], and consistency was demonstrated between simulated and measured results. The geometry of the probe was created by measuring the size of conductors and insulator with a calliper. The diameter of the inner conductor is 0.5 mm, the width of the insulator is 0.5 mm, and the width of the outer conductor is 0.35 mm. The material of the inner and outer conductors was assumed to be nickel, and the material of the insulator was assumed to be Teflon. As specified in [19], since the materials of the probe are unavailable to researchers, different combinations of materials were previously tested. Among the tested materials, nickel and Teflon are the materials that ensure the best match between simulated and measured dielectric properties [19].

The dielectrically interrogated samples were modelled as concentrically heterogeneous biological tissues consisting of a cylindrical inner tissue with variable radius ranging from 0.1 to 3 mm, surrounded by a concentric outer tissue that extends to a radius beyond that of the probe radius (i.e., beyond 1.1 mm). The diagram schematising the geometry of the simulation models is reported in Fig. 1. In the figure, the probe is shown in contact with the investigated sample, illustrated in grey with a red contour. The inner tissue is represented in blue with arrows indicating its variable size, and the surrounding outer tissue is illustrated in yellow. The discrete radii of the inner tissue were selected based on the results obtained from simulations performed in [18], [19]. In fact, in [19], it was found that the sensing radius can be smaller than the probe radius, and, in [18], simulations confirmed that the maximum sensing radius is approximately as large as the probe radius (i.e., 1.1 mm). Thus, the value of 3 mm chosen for the maximum radius of the inner tissue allows a margin of error above the previous maximum sensing radius estimate, and ensures that the sensing radius falls within this distance.

Once the simulation models were designed, various tissue combinations were examined in order to span different magnitudes and contrasts in permittivity. Specifically, 15 different tissues were combined into 38 distinct simulated samples. For each concentrically heterogeneous sample, an average of 20 simulations were planned (spanning different radii of inner tissue from 0.3 to 3 mm), for a total of about 760 simulations. The relative permittivity and conductivity of each of the 15 tissues were obtained from the IT'IS database [25]. In Fig. 2, the relative permittivity is plotted for all of the selected tissues. As is clear from Fig. 2, the 15 tissues span a wide range of

relative permittivity values. In fact, the average tissue relative permittivity ranges from 10.4 up to 77.2, across our frequency range of interest. Although the selected combinations of tissues are not practically significant, they cover the full spectrum of dielectric properties of biological tissues.

We also note that tissue sample compositions involving both healthy tissues and the corresponding malignant tissues would be of interest to investigate. However, to date, data on the dielectric differences between healthy and malignant tissues are known only for limited tissue types, such as liver, kidney and lung, and across restricted frequency ranges [11], [12].

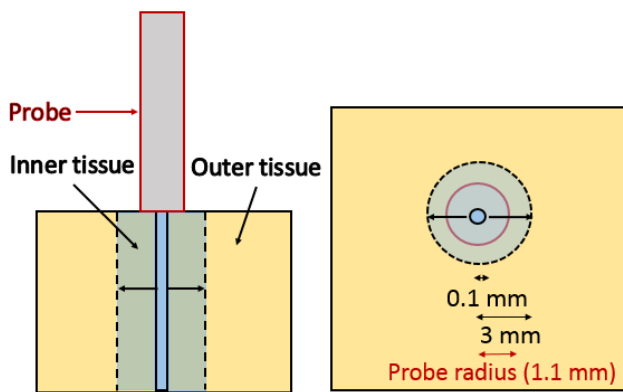


**FIGURE 1.** Diagram schematising the geometry of the simulation models developed for estimating the sensing radius. On the left, is a side view and, on the right, is a top view of the coaxial probe in contact with the concentrically heterogeneous sample. In both views, the probe position is illustrated in grey with a red contour, the inner tissue in blue, and the outer tissue in yellow. The variable size of the inner tissue radius is specified with arrows starting from the solid black lines and reaching the dotted black lines that delineate, respectively, the minimum and maximum size of the inner tissue, the radius of which ranges from 0.1 mm to 3 mm.

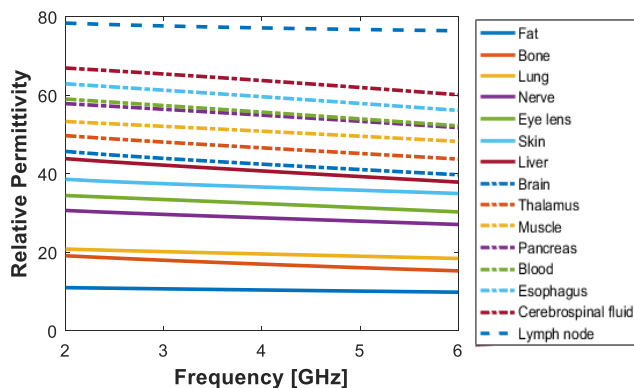


**FIGURE 2.** Relative permittivity of the 15 biological tissues selected for the simulated samples.

Since the sensing radius may depend on the contrast in permittivity between the two concentric tissues, it was also ensured that the 38 concentrically heterogeneous samples were composed of tissues spanning a wide range of contrasts. In this paper, the contrast in relative permittivity is defined as the percent difference in relative permittivity between the two tissues constituting the sample. Thus, the

contrast in relative permittivity between the two tissues was estimated as:

$$\Delta\epsilon_{r\%} = \frac{\epsilon_{r,\max} - \epsilon_{r,\min}}{\epsilon_{r,\max}} \times 100, \quad (1)$$

where  $\epsilon_{r,\max}$  is the relative permittivity of the constituent tissue with the highest relative permittivity and  $\epsilon_{r,\min}$  is the relative permittivity of the other constituent tissue (thus, having lower relative permittivity). The quantities  $\epsilon_{r,\max}$  and  $\epsilon_{r,\min}$  can refer to relative permittivity values at single frequencies or to mean relative permittivity values averaged across the simulation frequency range (2 - 6 GHz). The contrast in relative permittivity averaged across frequency varies between 7.4%, for the sample composed of muscle and pancreas, up to 86.5%, for the sample composed of fat and lymph node. As an example, the calculation of these two extreme contrasts is reported in the following paragraph.

Muscle and pancreas have average relative permittivities of 50.8 and 54.9, respectively. Alternatively, fat and lymph node have average relative permittivities of 10.4 and 77.2, respectively. Thus, the contrast in relative permittivity between muscle and pancreas (7.4%) is calculated as follows:

$$\frac{54.9 - 50.8}{54.9} \times 100,$$

and the contrast in relative permittivity between fat and lymph node (86.5%) is obtained as:

$$\frac{77.2 - 10.4}{77.2} \times 100.$$

Once the design of the study was completed, simulations were conducted using COMSOL Multiphysics. Simulation set-up and data post-processing details are reported in [18]. The relative permittivity and conductivity data obtained from each set of simulations were processed and analysed to calculate the sensing radius across all 38 scenarios, as reported in the following subsection.

## B. SENSING RADIUS CALCULATION AND ANALYSIS

The sensing radius was calculated for each of the 38 simulation scenarios across all frequencies between 2 and 6 GHz. For each scenario, the data from the simulation set schematised in Fig. 1 (involving the concentrically heterogeneous sample composed of an inner tissue of variable size surrounded by an outer tissue) was analysed. The sensing radius was calculated as the radius at which the outer tissue ceases to contribute to the dielectric properties, within the uncertainty of 2.5% (i.e., the distance at which only the permittivity of the inner tissue is detectable, within the uncertainty of 2.5%).

The choice of this uncertainty value is effectively arbitrary. In this case, 2.5% has been chosen as it is the uncertainty calculated from the experimental dielectric measurements system (described in detail in the following subsection). However, higher uncertainty values can be obtained for most of biological tissue dielectric data [8]. As discussed in previous works, different values of uncertainty can result in different values of sensing volume [26]. As

such, the choice of the uncertainty value can impact the size of the sensing radius. However, in this study, the sensing radius is calculated across all the 38 simulation scenarios only for comparison. Thus, the selected uncertainty does not affect the trend of the sensing radius across varying tissue constituents and contrasts. In fact, the uncertainty has the same weight on the quantitative estimation of the sensing radius across all the scenarios.

The sensing radius values obtained across all simulation scenarios were compared for each frequency point, since it is known that the sensing radius depends on the frequency [18], [27]. Also, for each scenario, the sensing radius was averaged across the frequency range, and it was observed that the average sensing radius was approximately equivalent to the sensing radius estimated for the central simulation frequency (4 GHz). In addition, it was determined that variations of the sensing radius with frequency were due primarily to differences in the dielectric contrast between the two concentric tissues across the frequency range. For instance, if the dielectric contrast between the tissues increases with the frequency, so does the sensing radius.

In the next section, the average sensing radius values are reported for each of the 38 scenarios. Specifically, only results referring to relative permittivity data are illustrated in Section III, since similar trends were also observed for conductivity. For an enhanced interpretation of these results, the sensing radius values were divided in three different categories based on the tissue composition of the simulated samples. The three categories involve: i) samples having same outer tissue, but different inner tissues; ii) samples having same inner tissue, but different outer tissues; iii) samples consisting of the same two tissues, but with swapped locations. Finally, the data from each category was interpolated with polynomial curves and then compared.

Before introducing the numerical results, the experimental set-up and measurement methodology designed to support the numerical outcome are described in the following subsection.

### C. APPLICABILITY OF THE NUMERICAL OUTCOME ON ANIMAL TISSUE DIELECTRIC MEASUREMENTS

Dielectric measurements were conducted to confirm the applicability of the numerical outcome in realistic scenarios. Specifically, the sensing radius calculated numerically was taken into account before conducting measurements in order to confirm that a tissue beyond the calculated sensing radius does not have any effect on the measured dielectric signal.

Dielectric measurements were performed using the Keysight slim form probe connected to the Agilent E5063A network analyser. The probe was calibrated using the three-load standard procedure. Before each set of measurements the quality of the calibration was verified by measuring the dielectric properties of 0.1 M NaCl, a standard reference liquid [28], [29]. The temperature of the calibration and

validation liquids were recorded during each dielectric measurement. Recordings of 0.1 M NaCl confirmed the measurement uncertainty was consistently around 2.5%. For each liquid/tissue measurement, the relative permittivity and conductivity were acquired at 51 frequency points on a linear scale over the frequency range of 2 - 6 GHz.

During tissue measurements, each sample was brought to the probe tip using a lift table, a firm contact between the probe and the tissue was kept, excess blood on the surface was removed by cotton swabs, and the tissue temperature was measured with an infrared thermometer. Furthermore, tissue dehydration was minimised by limiting the exposure of each sample to the air. Prior to measurements, tissue samples were kept in hermetically closed containers.

For this experimental validation, ovine heart samples were obtained from a local butcher. On the heart samples, small homogeneous tissue regions, approximately twice as large as the sensing radius calculated numerically, were identified. The size of the selected regions (approximately twice as large as the sensing radius calculated numerically) was chosen by considering that the sensing radius only delimits half of the sensing volume. On each small homogeneous tissue region, three measurements were taken and averaged. Between three and five measurements were also taken and averaged on larger homogeneous regions and then used as reference data.

An example of selected tissue sample area including small regions of a tissue surrounded by another type of tissue is provided in Fig. 3. The figure illustrates a lamb heart where fat tissue is well-distinguishable from muscle tissue. In Fig. 3, the area where measurements were performed is surrounded by a circle and, within that area, the fat/muscle interface is marked. Dielectric measurements were performed close to the marked fat/muscle interface, on both fat and muscle tissue regions, which were approximately twice as large as the sensing radius calculated numerically.



**FIGURE 3.** Lamb heart sample used to conduct dielectric measurements aimed at confirming the sensing radius calculated numerically. The area where measurements were performed is surrounded by a black circle and, within that area, the fat/muscle interface is marked.

Lastly, Cole-Cole models were fitted to the measured dielectric properties using the two-stage genetic algorithm [30]. The results from a subset of dielectric measurements performed on lamb heart are reported in Section III.C.

### III. RESULTS AND DISCUSSION

#### A. NUMERICAL SENSING RADIUS CALCULATION

In this subsection, an example demonstrating how the sensing radius was numerically calculated for each of the 38 simulation scenarios is provided.

In Fig. 4, the relative permittivity traces obtained for the simulation set involving the concentrically heterogeneous sample composed of esophagus as inner tissue and nerve as outer tissue are reported over 2 - 6 GHz. In Fig. 4, each trace corresponds to a given radius of the inner tissue (esophagus), as specified in the legend. From the relative permittivity plot, it is clear that as the esophagus radius increases, the relative permittivity values diverge from those of nerve and tend to those of the esophagus. In fact, when the radius of the esophagus tissue is 0.1 mm, the acquired relative permittivity values are, on average, only 3% different from the relative permittivity values of nerve (which has an average relative permittivity of 28.7). On the other hand, when the radius of the esophagus tissue is 3 mm, the acquired relative permittivity values are equivalent to those of esophagus (which has an average relative permittivity of 59.6) in isolation. The relative permittivity data in Fig. 4 were used for the calculation of the sensing radius for this sample composed of esophagus as inner tissue and nerve as outer tissue.

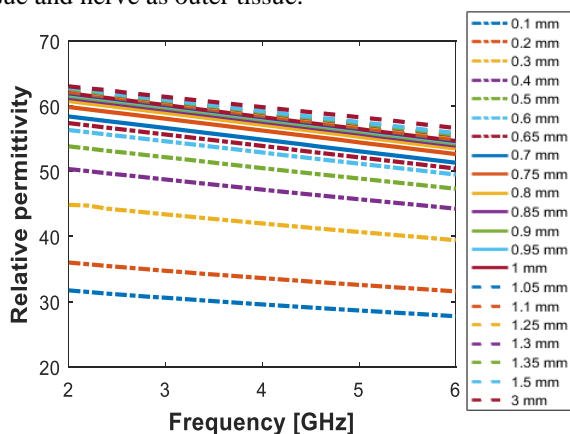


**FIGURE 4.** Relative permittivity traces obtained for the simulation set involving the concentrically heterogeneous sample composed of esophagus as inner tissue with variable radius and nerve as outer tissue. In the legend, the radius of the inner tissue (esophagus), ranging from 0.1 mm to 3 mm, is specified. As the radius of the esophagus tissue increases, the relative permittivity diverges from that of nerve (with average relative permittivity of 28.7) and tends toward that of the esophagus (with average relative permittivity of 59.6).

The sensing radius for each concentric sample was calculated by comparing the relative permittivity from simulations with differing inner tissue radii to the relative permittivity from the single simulation in which the inner tissue has a radius of 3 mm. The 3 mm radius is the maximum inner tissue size in each simulation set, and is representative of the probe measuring the inner tissue in

isolation. Thus, the relative permittivity obtained when the inner tissue radius is 3 mm was used as reference data for each simulation scenario. In particular, for each sample, the percent difference in relative permittivity between data from each of the simulations with variable inner tissue radius and the reference data was calculated across the frequency range. Then, to estimate the average sensing radius, the percent difference in relative permittivity was averaged across frequency. Fig. 5 illustrates the calculation of the average sensing radius for the sample composed of esophagus as inner tissue and nerve as outer tissue.

In the plot, each marker represents the average percent difference in relative permittivity between each of the traces in Fig. 4 and the trace corresponding to the simulation sample having esophagus radius of 3 mm (reference trace). In Fig. 5, it is clear that the average percent difference in relative permittivity decreases as the esophagus radius increases. As mentioned in Section II.B, the sensing radius corresponds to the radius of the inner tissue (esophagus) at which the measured permittivity of the heterogeneous sample differs by 2.5% (i.e., the measured uncertainty value) from the reference data permittivity. Specifically, in this scenario, with esophagus as inner tissue and nerve as outer tissue, a sensing radius of 1.05 mm was found.

Different values of sensing radius were obtained for different scenarios. The average sensing radii are analysed in the following subsection.

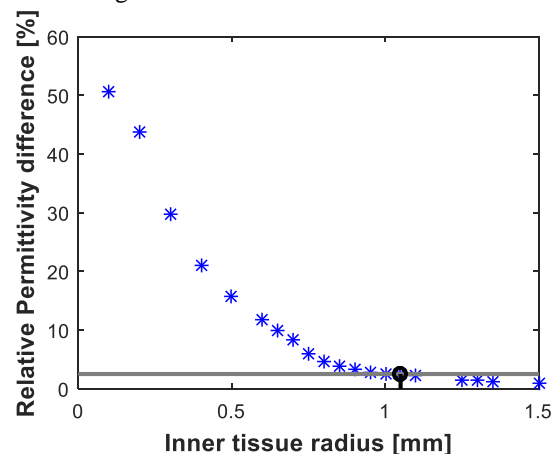


**FIGURE 5.** Plot of the percent difference in relative permittivity between the average relative permittivity (across frequency) from each simulation and the average relative permittivity (across frequency) from the simulation with the inner tissue having a radius of 3 mm (reference data), for the sample composed of esophagus as inner tissue and nerve as outer tissue. The sensing radius, calculated as the radius at which the outer tissue (nerve) ceases to contribute to the dielectric properties, within the uncertainty of 2.5%, is 1.05 mm, and is indicated with a vertical black line.

#### B. NUMERICAL SENSING RADIUS ANALYSIS

In this subsection, the results regarding the dependence of the sensing radius on the magnitude of the relative permittivity of the two concentric tissues, and their contrast, are reported. Then the sensing radius data, organised in the three categories (listed at the end of Section II.B), are analysed.

### B.1. Dependence of sensing radius on tissue permittivities and their contrast

In order to examine the trend of the sensing radius with varying relative permittivities of the constituent tissues, in Fig. 6, the average sensing radii calculated across the 38 scenarios are plotted versus the average relative permittivities of the inner and outer tissues of the corresponding concentric samples. In the 3D plot, two different trends were detected and organised in two clusters. The two clusters are related to the magnitude of the average relative permittivity of the inner tissue compared to that of the outer tissue. Specifically, in Fig. 6, the cluster representing samples composed of an inner tissue with relative permittivity lower than that of the outer tissue is indicated in blue, and the cluster representing the samples composed of an inner tissue with relative permittivity higher than that of the outer tissue is indicated in red. From the trend of the blue cluster, the sensing radius generally increases with the relative permittivity of the outer tissue; while, from the trend of the red cluster, the sensing radius also generally increases with the relative permittivity of the inner tissue.

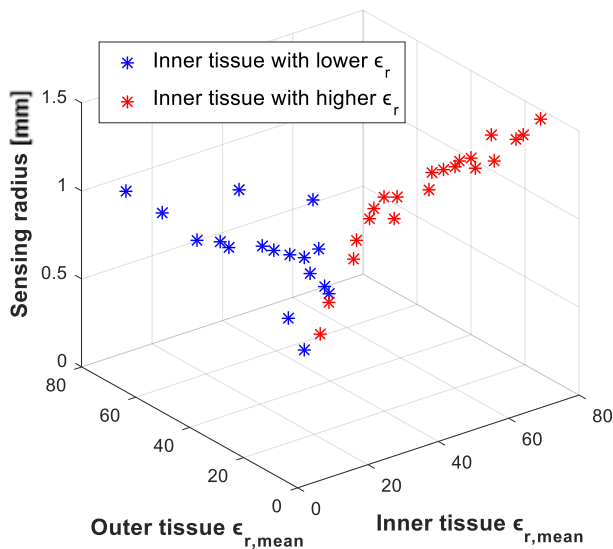


**FIGURE 6.** 3D plot of the average sensing radii from all simulation scenarios vs the average relative permittivities of the inner and outer tissues constituting each concentric sample. Two different clusters were identified: the cluster including samples composed of an inner tissue with relative permittivity lower than that of the outer tissue is indicated in blue, and the cluster of samples composed of an inner tissue with relative permittivity higher than that of the outer tissue is indicated in red.

In order to understand the trend of the sensing radius according to the contrast in relative permittivity between the two tissues constituting each sample, the sensing radius is next plotted versus the percent contrast in relative permittivity in Fig. 7. As is clear in Fig. 7, the two clusters, interpolated with linear polynomials, have similar trends, although the corresponding sensing radius values are lower for the samples with inner tissues having lower relative permittivity than for the samples with inner tissues having higher relative permittivity. However, for both clusters, the

sensing radius increases as the contrast in relative permittivity increases.

From Fig. 7, it is also clear that the average sensing radius varies from 0.3 mm and 1.5 mm, depending on the tissues present and their relative positions within the sample. The minimum and maximum sensing radii found correspond, respectively, to the samples composed of concentric tissues having the minimum and maximum contrast in relative permittivity. As specified at the end of Section II.A, the minimum contrast in relative permittivity was found for the sample consisting of muscle and pancreas, and the maximum contrast in permittivity was found for the sample consisting of fat and lymph node. Thus, the average sensing radius of 0.3 mm (the minimum sensing radius) is for the sample composed of muscle as inner tissue and pancreas as outer tissue, and the corresponding data in Fig. 7 is represented by the leftmost blue marker (this marker is part of the blue cluster, since the average relative permittivity of muscle is lower than that of pancreas). Similarly, the average sensing radius of 1.5 mm (the maximum sensing radius) is found for the sample composed of lymph node as inner tissue and fat as outer tissue, and the corresponding data in Fig. 7 is represented by the red marker on the extreme right (this marker is part of the red cluster, since the average relative permittivity of lymph node is higher than that of fat).

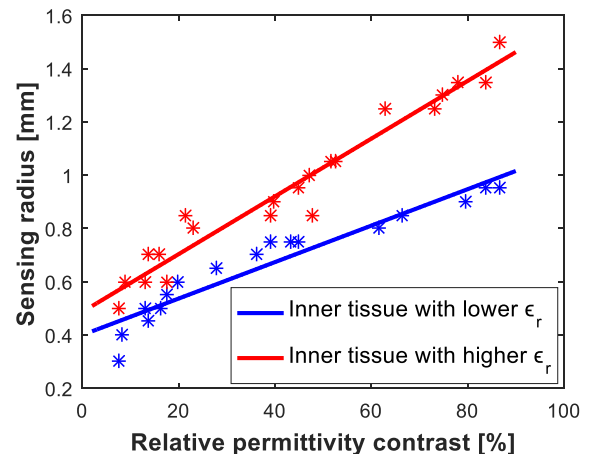


**FIGURE 7.** Sensing radius vs contrast in relative permittivity for the two clusters identified in Fig. 6: the blue cluster consisting of the samples with an inner tissue having lower relative permittivity, and the red cluster consisting of the samples with an inner tissue having higher relative permittivity. The plot also shows the linear polynomials interpolating the two data subsets (in solid traces).

In addition, it is of note that the maximum sensing radius calculated in this study (1.5 mm) is larger than the maximum histology radius estimated in [18], which was approximately as large as the probe radius (i.e., 1.1 mm). This difference in the estimated maximum sensing radius between these studies is due to the different uncertainty used for the calculation of the sensing radius. As mentioned in Section II.B, different uncertainty values can result in different values of sensing radius [26]. In fact, while in this study an uncertainty of 2.5% was considered, in [18] the total combined uncertainty of 4.2% was used for the

calculation of the sensing radius. Therefore, the results found in this study are consistent with those in [18].

Furthermore, the results obtained from these sets of simulations are consistent with the outcome of the study in [10]. In [10], the sensing radius of a coaxial probe was calculated by simulating the interaction of the probe with a sample composed of Teflon surrounded by a metal plate. The sample made of Teflon and metal represents the worst case scenario in terms of permittivity contrast, and thus enables the estimation of the maximum sensing radius of the probe. By considering the differences in probe dimension between this study and the study in [10], the maximum value of sensing radius of this study (i.e., 1.5 mm) is within the maximum sensing radius estimated in [10] (i.e., 1.55 mm).

### B.2. Dependence of sensing radius on inner tissue permittivity

In this subsection, the data from the three categories (samples having same outer tissue, but different inner tissue; samples having same inner tissue, but different outer tissue; and samples consisting of the same two tissues, but with swapped locations) are analysed and modelled.

In Fig. 8, the average sensing radius calculated across the scenarios consisting of samples having same outer tissue but different inner tissues is plotted versus the average relative permittivity of the inner tissue. For all scenarios plotted in Fig. 8, muscle is the outer tissue. Also in the plot of Fig. 8, two trends are detected and the data is distinguished into two clusters as in Fig. 6 and Fig. 7. Also in this case, the clusters refer to the average relative permittivity of the inner tissue with reference to the average relative permittivity of the outer tissue. In Fig. 8, the data corresponding to the scenarios with inner tissues having relative permittivity lower than that of muscle is illustrated in blue, and the data corresponding to inner tissues having relative permittivity higher than that of muscle is illustrated in red. In Fig. 8, the trends of the two clusters are delineated by two second degree polynomial curves that interpolate the two data subsets. From both trends, it is clear that the sensing radius is lower when the average relative permittivity of the inner tissue is closer to the average relative permittivity of muscle, i.e., 50.8. Furthermore, it is found that the sensing radius increases as the average relative permittivity of the inner tissue diverges from that of muscle.

Next, in Fig. 9, examples of results from the category of samples having the same inner tissue but different outer tissues are plotted. Specifically, the sensing radius versus the relative permittivity of the outer tissue is shown, for data from two clusters. One cluster refers to samples having fat as inner tissue with a range of other tissues as outer tissue (in blue) and the other cluster refers to samples having lymph node as inner tissue with a range of other outer tissues (in red). The two clusters have opposite trends, since the corresponding inner tissues, fat and lymph node, have very different relative permittivities which delimit the range of relative permittivity values of the tissues selected

for this study (as shown in Fig. 2). Specifically, the average relative permittivity of fat is 10.4, and the average relative permittivity of lymph node is 77.2. As such, the data from samples having fat as inner tissue are part of the cluster of samples with inner tissues having lower relative permittivity, and, vice versa, the data from samples having lymph node as inner tissue are part of the cluster of samples with inner tissues having higher relative permittivity than the outer tissues. In fact, in one case, fat has an average relative permittivity lower than that of all the outer tissues, and in the other case, lymph node has an average relative permittivity higher than that of all the outer tissues.

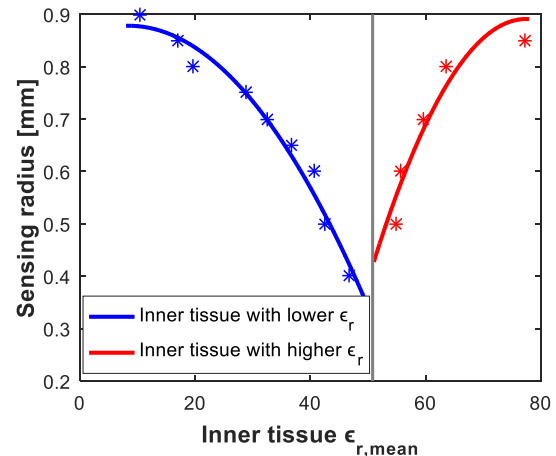


**FIGURE 8.** Plot of the average sensing radius vs average relative permittivity of the inner tissue for scenarios consisting of samples having the same outer tissue, i.e., muscle, but different inner tissues. The average relative permittivity of muscle (50.8) is marked with a grey vertical line in the plot and separates the data into two clusters: on the left, in blue, the cluster including samples composed of an inner tissue with relative permittivity lower than that of muscle, and, on the right, in red, the cluster composed of an inner tissue with relative permittivity higher than that of muscle. The data from the two clusters show different trends. To better define the trends, the two data subsets were interpolated with second degree polynomials. From both trends, it is clear that the sensing radius is lower when the average relative permittivity of the inner tissue is closer to that of muscle.

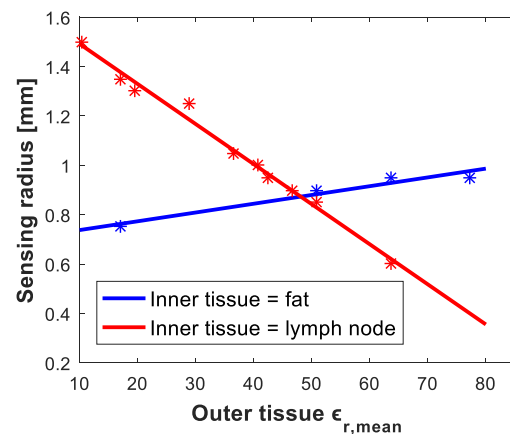


**FIGURE 9.** Sensing radius vs outer tissue relative permittivity for two clusters corresponding to the category of samples having the same inner tissue, but different outer tissues. The data in blue refers to samples having fat as inner tissue with a range of other tissues as outer tissue, and the data in red refers to samples having lymph node as inner tissue with a range of other outer tissues. The two clusters have different trends, since in one case, fat has an average relative permittivity lower than that of all the outer tissues, and in the other case, lymph node has an average relative permittivity higher than that of all the outer tissues.

Although the two subsets show opposite trends in Fig. 9, they present same trends in the sensing radius versus relative permittivity contrast plot in Fig. 10. In both cases, the sensing radius increases as the contrast in relative permittivity increases. In addition, as in Fig. 7, the sensing radius values are lower for the samples having fat as inner tissue (i.e., samples with the lower relative permittivity inner tissue) than for the samples having lymph node as inner tissue (i.e., samples with the higher relative permittivity inner tissue).

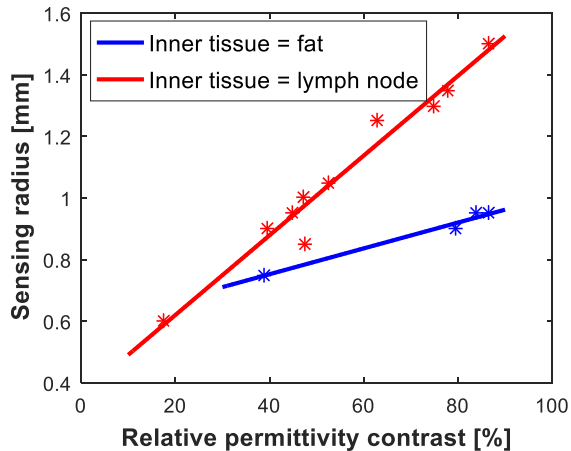


FIGURE 10 Sensing radius vs relative permittivity contrast for the two clusters illustrated in Fig. 9. For both clusters, the sensing radius increases with the contrast in relative permittivity.

In Fig. 11, the average sensing radius from three couplets of datasets corresponding to the category of samples composed of the same tissues but with swapped location are plotted versus the average relative permittivity of the inner tissue. One couplet refers to the two samples composed of fat and lymph node (in blue), another couplet refers to the two samples composed of cerebrospinal fluid and lymph node (in red), and the last refers to the two samples composed of brain and lymph node (in green). The three couplets of datasets show similar trends, although they have different contrasts in relative permittivity. Specifically, the sample composed of fat and lymph node has the highest contrast in relative permittivity (86.57%), the sample composed of cerebrospinal fluid and lymph node has the lowest contrast in relative permittivity (17.59%), and the sample composed of brain and lymph node has a contrast in relative permittivity of 44.96%. From Fig. 11, it can be observed that the higher the contrast between the two tissues, the higher the difference in sensing radii between the two samples within a couplet. Furthermore, in each couplet, the lowest sensing radius corresponds to the case with the lower permittivity tissue occupying the inner region of the concentric sample. Similarly, the highest sensing radius corresponds to the case with the higher permittivity tissue occupying the inner region of the concentric sample. The outcome of these case scenarios confirms the outcomes previously reported in Section III.B.1. In fact, across the three data categories, it was

confirmed that the permittivity of the inner tissue has a great impact on the sensing radius, and that the sensing radius increases with the contrast in permittivity between the two concentric tissues.

In the next subsection, experimental results are reported to validate the numerical outcome across a subset of measurement scenarios.

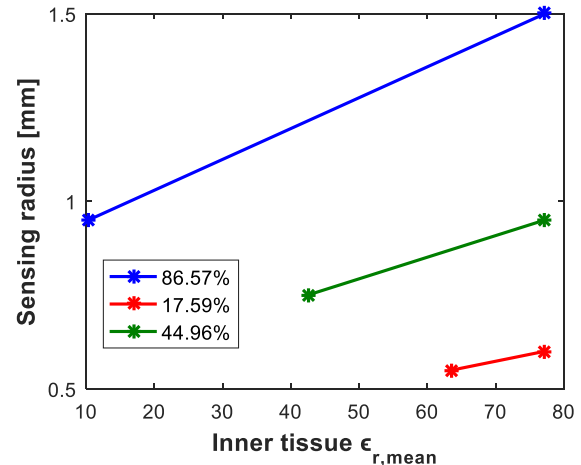


FIGURE 11. Sensing radius vs inner tissue relative permittivity for three couplets of datasets corresponding to the category of samples having same tissues but with the locations swapped. The two tissues from each couplet have different percent contrasts in relative permittivity, which are reported in the legend. The data in blue is from the sample composed of fat and lymph node, the data in red is from the sample composed of cerebrospinal fluid and lymph node, and the data in green is from the sample composed of brain and lymph node. In each couplet, the lowest sensing radius corresponds to the case of the lower permittivity tissue occupying the inner region of the concentric sample.

### C. VALIDATION OF THE NUMERICAL OUTCOME ON ANIMAL TISSUE DIELECTRIC MEASUREMENTS

In this subsection, dielectric data obtained from measurements on lamb heart samples is analysed and discussed.

All measured heart samples were composed of both fat and muscle. An average contrast in relative permittivity of 80% between heart muscle and fat was obtained across all measured samples. Considering the numerical outcome summarised in Fig. 8, if the contrast between two tissues is around 80%, then the sensing radius is approximately 0.9 mm, for the case of fat surrounded by heart muscle, and 1.3 mm, for the case of heart muscle surrounded by fat. Thus, on each heart sample, after measuring the dielectric properties of large homogeneous tissue regions to use as reference data, three dielectric measurements were taken on small muscle regions that were approximately 2.6 - 3 mm wide and on small fat regions that were approximately 1.8 - 2.2 mm wide. The data acquired from each region was averaged and then one pole Cole-Cole model was fitted to each dielectric trace. Lastly, the data acquired from small heart muscle and fat tissue regions, was compared with the fat and muscle data acquired from the larger sample regions.

In Fig. 12, the fitted Cole-Cole models obtained across the area of the sample illustrated in Fig. 3 are shown.

Specifically, one pole Cole-Cole model was fitted to the measured data from small and large heart muscle regions, and small and large fat regions. The parameters of each Cole-Cole model are summarised in Table I. The average fractional error between the measured data and the fitted model in all four cases was less than 0.6%.

In Fig. 12, the reference data from [31] are also reported. The measured heart muscle and fat dielectric properties are consistent with the data from the literature. The average measured data is approximately 4% higher than the data from the literature, and this difference can be attributed to the presence of some blood on the surface of the sample, although, during the measurement, excess blood was removed with cotton swabs.

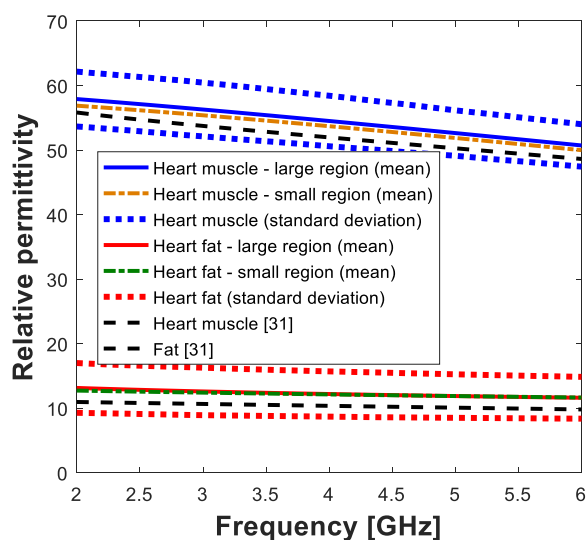


**FIGURE 12.** Plot of the relative permittivity of the fitted Cole-Cole model for each of the measurement regions, along with reference data from Gabriel et al. 1996 [31]. The blue and red solid traces refer to relative permittivity values measured from large heart muscle and fat homogeneous regions, respectively. The orange and green dash-dotted traces refer to relative permittivity values measured from small heart muscle and fat homogeneous regions, respectively. The small tissue regions were approximately twice as large as the sensing radius calculated numerically. In the plot, also the standard deviations obtained from heart muscle and fat tissues are reported.

**TABLE I**  
ONE POLE COLE-COLE MODEL PARAMETERS FOR LARGE AND SMALL TISSUE REGIONS FROM THE HEART SAMPLES

Parameters	Muscle (large)	Fat (large)	Muscle (small)	Fat (small)
$\epsilon_\infty$	5.96	1	11.34	2.53
$\Delta\epsilon$	54.42	17.76	47.54	11.21
$\tau$ (s)	9.52e-12	8.35e-12	1.07e-11	4.32e-12
$\alpha$	0.11	0.68	0.08	0.36
$\sigma_s$ (S/m)	0.95	0.12	0.99	0.21

From the plot in Fig. 12, the average relative permittivity obtained from small regions is less than 2% different from the average relative permittivity obtained from larger regions. This difference is within the measurement uncertainty (2.5%). Therefore, the tissue surrounding the small region does not have any dielectric impact on the measurement. Thus, the measurements confirm the numerical outcome and demonstrate that, within the sensing

radius calculated numerically, only the dielectric properties of the tissue of interest are actually measured.

Before concluding this paper, in the next subsection, the outcomes from numerical simulations and dielectric measurements are summarised, and their significance is highlighted.

#### D. DISCUSSION

Overall, two key observations can be concluded based on the results of the simulations reproducing the acquisition of dielectric properties from concentrically heterogeneous biological tissues with the Keysight slim form probe.

Firstly, the permittivity of the inner tissue greatly impacts the acquired signal and, as a consequence, it affects also the value of the sensing radius. Specifically, the higher the permittivity of the inner issue, the higher the estimated sensing radius. This outcome confirms the findings in [18], [19], where it was observed that tissues constituting concentrically heterogeneous samples have a different impact on the acquired dielectric properties, depending on their location (i.e., depending whether the tissue occupies the inner or outer region of the concentric sample). In particular, in both studies, it was found that the inner tissue has a significantly higher impact on the acquired dielectric properties when its permittivity is lower than that of the outer tissue. Additionally, in [19], a sensing radius of 0.9 mm was estimated for a concentric sample having fat as inner tissue and muscle as outer tissue, and a sensing radius of 1 mm was estimated for the concentric sample having muscle as inner tissue and fat as outer tissue. Thus, the outcome in [19] confirms that, for concentric samples having an inner tissue with higher permittivity (i.e., muscle), the sensing radius is higher than for concentric samples having an inner tissue with lower permittivity (i.e., fat).

Secondly, it was observed that the sensing radius increases with the contrast in permittivity between the two concentric tissues. Across all scenarios spanning different permittivities and contrasts, sensing radius values ranging from 0.3 to 1.5 mm were obtained. The minimum value of sensing radius (0.3 mm) was calculated from the concentric sample having muscle as inner tissue and pancreas as outer tissue. This sample has the minimum contrast in permittivity and has a lower permittivity tissue as the inner tissue (since the average relative permittivity of muscle is 50.8 and the average relative permittivity of pancreas is 54.9). Inversely, the maximum sensing radius value was obtained for the concentric sample having lymph node as inner tissue and fat as outer tissue, which is the sample with the maximum contrast in permittivity and the highest permittivity tissue as inner tissue (since the average relative permittivity of lymph node is 77.2 and the average relative permittivity of fat is 10.4).

Lastly, the results obtained from dielectric measurements confirmed that, within the sensing radius calculated numerically, only the tissue of interest is measured. In this way, the applicability of the numerical outcome for the

dielectric characterisation of biological tissues has been validated.

It is of note that the quantitative results obtained in this study are only valid for the Keysight slim form probe, since the sensing radius depends on the geometry and features of the probe used. However, the trend of the sensing radius, depending on the dielectric properties of the interrogated tissues, can be extended to any type of probe.

In summary, these findings highlight the importance of taking into account the dielectric properties of the constituent tissues of the investigated sample when estimating the sensing radius. The estimation of the sensing radius is fundamental to define the minimum width of the homogeneous tissue region that ensures accurate tissue dielectric measurements.

Finally, accurate dielectric characterisation of biological tissues supports the design of the EM medical technologies.

#### IV. CONCLUSIONS

In this study, numerical simulations conducted on concentric heterogeneous biological samples demonstrated that the sensing radius of a coaxial probe depends strongly on the dielectric properties of both the inner and outer tissues constituting the concentric sample. Then, the numerical outcome was validated with dielectric measurements on animal tissues.

First, it was found that the inner tissue greatly impacts the size of the sensing radius. Based on the magnitude of the permittivity of the inner tissue relative to that of the outer tissue, two different trends in sensing radius were detected. In particular, the sensing radius values were found to be lower when the permittivity of the inner tissue was lower than that of the outer tissue. On the other hand, the sensing radius values were higher when the permittivity of the inner tissue was higher than that of the outer tissue.

It was also observed that the sensing radius trend varies with the contrast in permittivity between the two concentric tissues. In general, the higher the contrast, the higher the sensing radius.

In summary, in this study, the dependence of the sensing radius on the dielectric properties of the interrogated tissue was investigated. The estimation of the sensing radius supports the definition of the minimum width of the homogeneous tissue required to measure only the tissue of interest and no other surrounding tissue within heterogeneous samples

The outcomes of this study are the foundation for a rigorous estimation of the sensing radius, which supports accurate dielectric measurement of biological tissues. Accurate dielectric characterisation of biological tissues has the potential to improve the design and use of EM medical technologies, such as MW imaging and ablation.

#### ACKNOWLEDGMENT

This work has been developed in the framework of COST Action MiMed (TD1301).

#### REFERENCES

- [1] M. Pastorino, *Microwave imaging*. John Wiley & Sons, 2010.
- [2] R. J. Halter *et al.*, "The correlation of in vivo and ex vivo tissue dielectric properties to validate electromagnetic breast imaging: initial clinical experience," *Physiol. Meas.*, vol. 30, no. 6, pp. S121–S136, 2009.
- [3] M. Ahmed, C. L. Brace, F. T. Lee, and S. N. Goldberg, "Principles of and advances in percutaneous ablation," *Radiology*, vol. 258, no. 2, pp. 351–369, 2011.
- [4] V. Lopresto, R. Pinto, L. Farina, and M. Cavagnaro, "Treatment planning in microwave thermal ablation: clinical gaps and recent research advances," *Int. J. Hyperth.*, vol. 33, no. 1, pp. 83–100, 2017.
- [5] A. La Gioia *et al.*, "Open-Ended Coaxial Probe Technique for Dielectric Measurement of Biological Tissues: Challenges and Common Practices," *Diagnostics*, vol. 8, no. 40, pp. 1–38, 2018.
- [6] T. W. Athey, M. A. Stuchly, and S. S. Stuchly, "Measurement of radio frequency permittivity of biological tissues with an open-ended coaxial line: Part I," *IEEE Trans. Microw. Theory Tech.*, vol. 30, no. 1, pp. 82–86, 1982.
- [7] S. Gabriel, R. W. Lau, and C. Gabriel, "The dielectric properties of biological tissues: II. Measurements in the frequency range 10 Hz to 20 GHz," *Phys. Med. Biol.*, vol. 41, no. 11, pp. 2251–2269, 1996.
- [8] A. Peyman, S. Holden, and C. Gabriel, "Mobile Telecommunications and Health Research Programme: Dielectric Properties of Tissues at Microwave Frequencies," 2005.
- [9] M. Lazebnik *et al.*, "A large-scale study of the ultrawideband microwave dielectric properties of normal, benign and malignant breast tissues obtained from cancer surgeries," *Phys. Med. Biol.*, vol. 52, no. 20, pp. 6093–6115, 2007.
- [10] P. De Langhe, L. Martens, and D. De Zutter, "Design Rules for an Experimental Setup Using an Open-Ended Coaxial Probe Based on Theoretical Modelling," *IEEE Trans. Instrum. Meas.*, vol. 43, no. 6, pp. 810–817, 1994.
- [11] W. T. Joines, Y. Zhang, C. Li, and R. L. Jirtle, "The measured electrical properties of normal and malignant human tissues from 50 to 900 MHz," *Med. Phys.*, vol. 21, no. 4, pp. 547–550, 1994.
- [12] A. Peyman *et al.*, "Variation in dielectric properties due to pathological changes in human liver," *Bioelectromagnetics*, vol. 36, no. 8, pp. 603–612, 2015.
- [13] G. Chen, K. Li, and Z. Ji, "Bilayered Dielectric Measurement With an Open-Ended Coaxial Probe," *IEEE Trans. Microw. Theory Tech.*, vol. 42, no. 6, pp. 966–971, 1994.
- [14] E. Alanen, T. Lahtinen, and J. Nuutinen, "Measurement of dielectric properties of subcutaneous fat with open-ended coaxial sensors," *Phys. Med. Biol.*, vol. 43, no. 3, pp. 475–485, 1998.
- [15] P. M. Meaney, A. P. Gregory, J. Seppälä, and T. Lahtinen, "Open-Ended Coaxial Dielectric Probe Effective Penetration Depth Determination," *IEEE Trans. Microw. Theory Tech.*, vol. 64, no. 3, pp. 915–923, 2016.
- [16] E. Porter and M. O'Halloran, "Investigation of Histology Region in Dielectric Measurements of Heterogeneous Tissues," *IEEE Trans. Antennas Propag.*, vol. 65, no. 10, pp. 5541–5552, 2017.
- [17] E. Porter, A. La Gioia, A. Santorelli, and M. O'Halloran, "Modeling of the Dielectric Properties of Biological Tissues within the Histology Region," *IEEE Trans. Dielectr. Electr. Insul.*, vol. 24, no. 5, pp. 3290–3301, 2017.
- [18] A. La Gioia, M. O'Halloran, A. Elahi, and E. Porter, "Investigation of Histology Radius for Dielectric Characterisation of Heterogeneous Materials," *IEEE Trans. Dielectr. Insul.*, vol. 25, no. 3, pp. 1065–1080 [In print], 2018.
- [19] A. La Gioia, S. Salahuddin, M. O'Halloran, and E. Porter, "Quantification of the Sensing Radius of a Coaxial Probe for Accurate Interpretation of Heterogeneous Tissue Dielectric Data," *IEEE J. Electromagn. RF Microwaves Med. Biol.*, vol. [In print], 2018.
- [20] Keysight, "N1501A Dielectric Probe Kit 10 MHz to 50 GHz: Technical Overview. Available at: <http://www.keysight.com/en/pd-2492144-pn-N1501A/dielectric-probe-kit>. [Accessed 30 October 2017].," 2015.
- [21] L. Abdilla, C. Sammut, and L. Mangion, "Dielectric properties

of muscle and liver from 500 MHz-40 GHz,” *Electromagn. Biol. Med.*, vol. 32, no. 2, pp. 244–252, 2013.

- [22] A. Martellosio *et al.*, “Dielectric properties characterization from 0.5 to 50 GHz of breast cancer tissues,” *IEEE Trans. Microw. Theory Tech.*, vol. 65, no. 3, pp. 998–1011, 2017.
- [23] A. P. O’Rourke *et al.*, “Dielectric properties of human normal, malignant and cirrhotic liver tissue: in vivo and ex vivo measurements from 0.5 to 20 GHz using a precision open-ended coaxial probe,” *Phys. Med. Biol.*, vol. 52, no. 15, pp. 4707–19, 2007.
- [24] V. Lopresto, R. Pinto, G. Lovisolo, and M. Cavagnaro, “Changes in the dielectric properties of ex vivo bovine liver during microwave thermal ablation at 2.45 GHz,” *Phys. Med. Biol.*, vol. 57, no. 8, pp. 2309–2327, 2012.
- [25] P. Haggall *et al.*, “IT’IS Database for thermal and electromagnetic parameters of biological tissues,” *Version 4.0*, 2018. [Online]. Available: [www.itis.ethz.ch/database](http://www.itis.ethz.ch/database).
- [26] E. Porter, A. La Gioia, A. Bottiglieri, and M. O’Halloran, “Challenges in the Dielectric Measurement of Heterogeneous Tissues: Impact of Uncertainty in Sensing Depth Calculation,” in *2nd URSI AT-RASC, Gran Canaria*, 2018.
- [27] D. Hagl, D. Popovic, S. C. Hagness, J. H. Booske, and M. Okoniewski, “Sensing volume of open-ended coaxial probes for dielectric characterization of breast tissue at microwave frequencies,” *IEEE Trans. Microw. Theory Tech.*, vol. 51, no. 4, pp. 1194–1206, 2003.
- [28] C. Gabriel and A. Peyman, “Dielectric measurement: error analysis and assessment of uncertainty,” *Phys. Med. Biol.*, vol. 51, no. 23, pp. 6033–6046, 2006.
- [29] A. Peyman, C. Gabriel, and E. H. Grant, “Complex permittivity of sodium chloride solutions at microwave frequencies,” *Bioelectromagnetics*, vol. 28, no. 4, pp. 264–274, 2007.
- [30] S. Salahuddin, E. Porter, F. Krewer, and M. O’Halloran, “Optimised analytical models of the dielectric properties of biological tissue,” *Med. Eng. Phys.*, vol. 43, pp. 103–111, 2017.
- [31] S. Gabriel, R. W. Lau, and C. Gabriel, “The dielectric properties of biological tissues: III. Parametric models for the dielectric spectrum of tissues,” *Phys. Med. Biol.*, vol. 41, no. 11, pp. 2271–2293, 1996.



**Dr. Emily Porter** received her B.Eng., M.Eng., and Ph.D. degrees in electrical engineering from McGill University, Montreal, Canada, in 2009, 2010, and 2015 respectively. Dr. Porter was a recipient of the 2013 IEEE Antennas and Propagation Society Doctoral Research Award for her work on breast health monitoring using a time-domain microwave system. Dr. Porter is currently an EU Marie-Curie Fellow with the Translational Medical Device Laboratory at the National University of Ireland Galway. Her current research interests include the measurement of dielectric properties of biological tissues and the development novel technologies for therapeutic and diagnostic applications of electromagnetic waves.



**Ms. Alessandra La Gioia** is a Ph.D. student in the Translational Medical Device Laboratory, funded by European Research Council and led by Dr. Martin O’Halloran, at National University of Ireland, Galway (NUIG). She completed her Bachelor’s and Master’s degrees in Biomedical Engineering at the University of Bologna (Italy) with first-class honours. Currently, she is investigating techniques for the analysis of the dielectric properties

of biological tissues, as a platform for low-cost medical device design.



**Dr. Martin O’Halloran** received a B.Eng. (Hons.) and Ph.D. in Engineering from the National University of Ireland Galway (NUIG) in 2004 and 2009, respectively. He also holds an MSc. in Clinical Research (2014), also from NUIG. Dr. O’Halloran is the Director of the Translational Medical Device Lab at NUIG, and is Director of Enabling Technologies at BioInnovate (an affiliate of Stanford’s BioDesign Programme).

He has over 25 national and international awards, including Engineers Ireland Engineer of the Year 2014, and Science Foundation Ireland’s EC Researcher of the Year 2016. Dr. O’Halloran’s research is funded by Science Foundation Ireland, the Irish Research Council and the European Research Council. His research is focused on patient-centered medical device design and development.